

Physical parameter and loss determination of piezoceramics using partial

electrode: k_{31} and k_{33} mode cases

Yoonsang Park^{1,*}, Hossein Daneshpajoo¹, Timo Scholehwar², Eberhard Hennig², and Kenji Uchino¹

1) International Center for Actuators and Transducers (ICAT), The Pennsylvania State University, University Park, PA, 16802, USA

2) R&D Department, PI Ceramic GmbH, Lindenstrasse, 07589 Lederhose, Germany

Abstract: The standard method to determine physical parameters of piezoceramics, established by IEEE, has been utilized for decades by the number of researchers, yet it omits presence of important loss factors and possesses serious deficits that restricts accurate parameter determination. In order to resolve these issues, the partial electrode (PE) method (mechanical excitation method) was previously proposed. In this study, we aim to propose a modified PE method to enhance the efficiency of parameter determination process, along with a simplified analytical admittance equation for better understanding of the PE configuration. To prove that the PE method is reliable, possible causes of errors were listed, and it was shown that they were either negligibly small or resolved with proper calibration methods. Throughout the paper, it was validated that the PE method not only reduces the errors of several physical parameters by avoiding error propagation, but also enables measurement compatibility with commercially available impedance analyzers.

Keywords: piezoelectric composite, loss determination method, piezoelectric loss, mechanical quality factor, heat generation

1. Introduction

High-power piezoelectric devices, such as ultrasonic transducers, actuators and voltage transformers, have been rigorously developed through recent decades[1-4]. The demand for miniaturization of high-power piezoelectric devices has grown rapidly[5,6], as the significance of micro-scale electronic devices are being emphasized. As such, piezoelectric devices have effectively replaced conventional electromagnetic counterparts with better performance and no electromagnetic noise[7-9]. As the demanding scales for electronic devices are getting smaller and smaller, further miniaturization of piezoelectric device is required. However, miniaturization of devices while maintaining energy density is still limited, due to heat generation that degrades the overall performance of high-power piezoelectric devices[7,8,10-13].

It is known that the heat generation is mainly due to “losses” in piezoelectric materials[7]. There are in general three types of losses: elastic, dielectric, and piezoelectric losses[14-16]. Those three categories are further classified as either intensive or extensive, based on specific electrical or mechanical boundary conditions. In terms of simplified 1D mathematical expression, we have[8,17,18]:

$$\varepsilon^{X*} = \varepsilon^X (1 - j \tan \delta') \quad (1)$$

$$s^{E*} = s^E (1 - j \tan \phi') \quad (2)$$

$$d^* = d (1 - j \tan \theta') \quad (3)$$

$$\kappa^{x*} = \kappa^x (1 + j \tan \delta) \quad (4)$$

$$c^{D*} = c^D (1 + j \tan \phi) \quad (5)$$

$$h^* = h (1 + j \tan \theta) \quad (6)$$

where ε^X is stress (X)-constant permittivity, s^E is “electric field (E)-constant” elastic compliance, d is piezoelectric coefficient, κ^x is strain (x)-constant inverse permittivity, c^D

is dielectric displacement (D)-constant elastic stiffness, and h is inverse piezoelectric coefficient. The former three parameters are named “intensive physical parameters”, while the latter three are called “extensive physical parameters”. The primed loss tangent values in imaginary part of each complex, (with superscripted stars) are “intensive loss”, whereas non-primed loss tangent values are “extensive” losses. The negative signs for intensive losses and positive signs for extensive losses are due to convention, considering the direction of loss hysteresis loop[8].

Each type of loss, either intensive or extensive, has its own significance. For example, intensive losses, as input parameters, greatly increase the accuracy of finite element analysis (FEA) computer simulation[19-21], which is a powerful tool to investigate desired targeting resonance frequency or mechanical quality factors of piezoelectric devices. Such a tool provides convenient way to design piezoelectric devices without actual fabrication. Meanwhile, extensive losses, losses in constrained boundary conditions, are helpful in elucidating heat generation mechanism due to domain wall dynamics[10,22]. Therefore, obtaining accurate values of both intensive and extensive losses are important, from both technological and scientific interests.

The standard method to determine physical parameters and losses was first established by IRE Standard[23], then further shaped by Institute for Electrical and Electronics Engineer (IEEE) in 1980s[24]. However, there are several deficits in this method that prevent users from obtaining accurate parameters. For example, according to the piezoelectric equivalent circuit (EC) described in IEEE Standard on Piezoelectricity, only one type of loss (elastic loss) is explained as a resistor in LCR circuit[24]. Therefore, until the first experimental demonstration of “piezoelectric loss” in 2000s[14], many researchers have believed that the quality factor at resonance frequency (Q_A) is equivalent to that at antiresonance frequency (Q_B). There are even more issues with IEEE Standard on piezoelectricity: for example, in k_{33} mode

(a bar with electric field parallel to sound velocity) specimen, shown in Figure 1 (b), high impedance values near antiresonance frequency is the most significant issue, and there are even more issues, such as wire attachment issues and electric flux leakage[18,25-27]. Furthermore, while k_{31} mode (a bar with electric field perpendicular to sound velocity) specimen, shown in Figure 1 (a), only provides intensive elastic loss originated from Q_A , k_{33} mode, shown in Figure 1 (b), only provides extensive-like (see subsection 3.2 for further explanation) elastic loss originated from Q_B . For each mode, in order to obtain other types of loss values (extensive in k_{31} and intensive in k_{33} mode), one has to utilize either $[K]$ matrix[8,10,17] or other complicated equations originated from piezoelectric constitutive relations[28], which dramatically increase error from standard deviation due to error propagation.

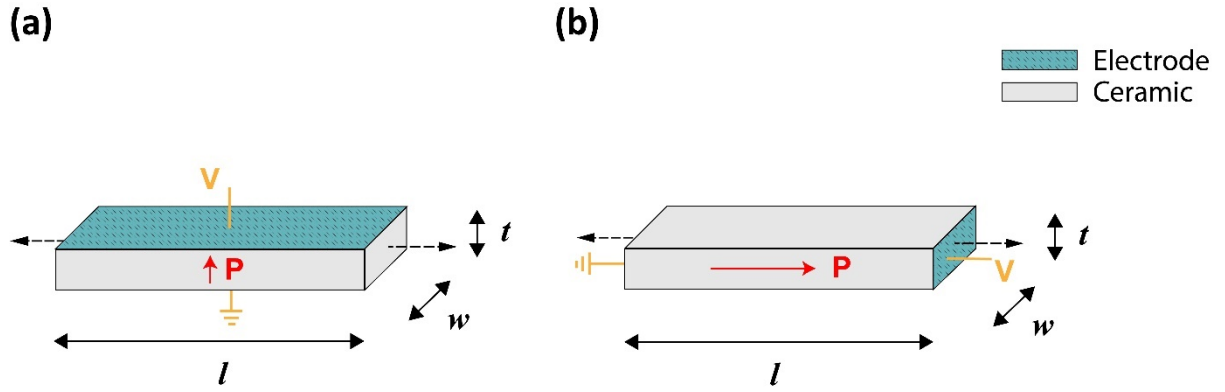


Figure 1. Standard (a) k_{31} mode and (b) k_{33} mode piezoelectric specimen. Voltage and polarization directions, as well as sample dimensions are defined. Redrawn from IEEE Standard on Piezoelectricity [20].

In order to resolve such issues, partial electrode (PE) method, which is basically a mechanical excitation method, was previously proposed[18,29], as shown in Figure 2. The PE configuration is composed of center part, which is electrically excited, and side part, which is mechanically excited by the center part. The advantage of PE is that intensive and extensive-like elastic compliances and losses can both be determined using the same configuration just

by changing the surface electrode. For example, the side with no electrode, as shown in Figure 2 (c), provides extensive-like elastic compliance and loss, whereas side with electrode, as shown in Figure 2 (d), provides intensive elastic compliance and intensive elastic loss. Furthermore, since the mechanical excitation of the side specimen can be monitored by impedance/admittance measurement with the center part, experimental impedance values are in the range of 10^4 and $10^5 \Omega$ for soft PZT[18,29]. Therefore, high impedance issue of the IEEE Standard k_{33} mode specimen can be resolved.

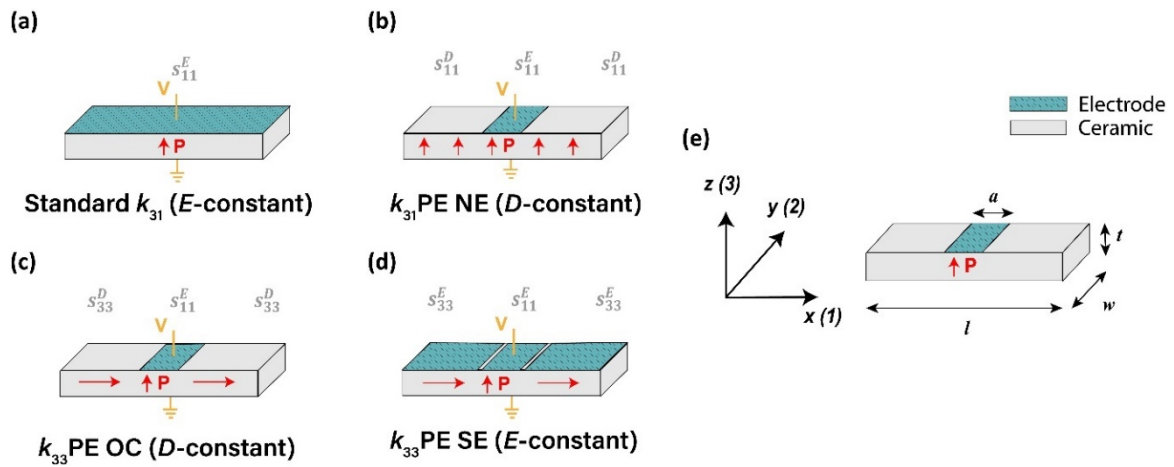


Figure 2. Sample geometries of (a) Standard k_{31} specimen, (b) k_{31} mode PE non-electrode (NE), (c) k_{33} mode PE open circuit (OC) and (d) k_{33} mode PE side electrode (SE) used in this study. Grey characters above each geometry denote corresponding elastic compliance to specific parts of geometry. (e) Coordinate and dimension definition of a PE sample.

In this study, we aim to provide detailed physical parameters and loss determination process using the PE method. Different from previous descriptions that included open circuit (OC) for antiresonance characterization and short circuit (SC) for resonance characterization[17,18], the number of types of PE configuration has been reduced for experimental simplicity. For determination of both intensive and extensive-like, real and

imaginary elastic parameters and other physical parameters (such as dielectric and piezoelectric parameters), the following 4 types of samples are needed: IEEE Standard k_{31} specimen, k_{31} PE non-electrode (NE), k_{33} PE open circuit (OC) and k_{33} PE side electrode (SE). Throughout the paper, the following materials will be discussed: simplified and universal admittance equation for PE configuration, possible error causes for PE method and comprehensive parameter determination process using PE samples.

2. Material and Methods

For 4 types of samples made from both PIC 255 (Nb-doped soft PZT) and PIC 181 (Mn-doped hard PZT) [PI Ceramic GmbH, Lederhose, Germany] (soft and hard PZT for checking the samples' performance difference), 6 samples with the dimension of length (l) \times width (w) \times thickness (t) = $20 \times 2.5 \times 0.5$ mm (See Figure 1 and 2 for dimension definition of samples) were prepared: IEEE Standard k_{31} specimen, k_{31} PE NE, k_{33} PE OC, and k_{33} PE SE. For all the samples, pure Ag was sputtered and used as electrode. For the PE samples, center electrode was maintained to about 10 % of the total l of the sample, and the portion of the center part for each PE sample was measured with optical microscope. The off-resonance (for permittivity measurement) and the fundamental mode on-resonance admittance/impedance spectra for each sample were measured with 4294A Precision Impedance Analyzer [Agilent Technologies, Santa Clara, CA], with 100 mV input voltage (low vibration velocity range for escaping from the heat generation). For Standard k_{31} mode, the parameter determination procedure described by Zhuang *et al.*[30] was utilized; for PE samples, experimental admittance curves were fitted to analytical equations derived in our previous work[18] to obtain elastic compliance and loss values. For each determined parameter, error was determined by using standard deviation divided by square root of measurement number, and error propagation

method was utilized for parameters that were calculated through the equations. Figure 3 shows actual piezoceramic samples used in this study.

ATILA++ Finite Element Method software (distributed by Micromechatronics Inc., State College, PA) was utilized in this study, in order to verify analytical admittance equations and to observe the effect of volumes with canted polarization (see section 4.1.4). Refer to supplementary materials for more information on FEA simulation.

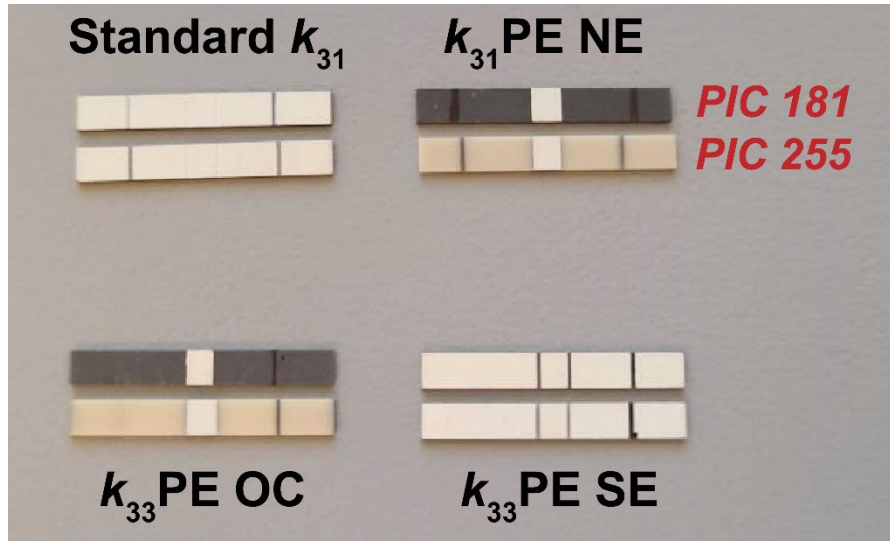


Figure 3. Actual piezoelectric samples used in this study. Black lines denote polarization direction; faces with 2 black lines represent positive side (arrowhead) of polarization. See Figure 1 and 2 for specific geometry of each sample.

3. Theory/Calculation

3.1 Parameter Determination Using Standard k_{31} Mode

Determination of physical parameters of Standard k_{31} specimen was already shown in IEEE Standard and Zhuang *et al.*[24,30]. The basic formulation starts from admittance equation, which is given by:

$$Y_{31}^* = j\omega \frac{\varepsilon_0 \varepsilon_{33}^{X*} w l}{t} \left[(1 - k_{31}^{*2}) + k_{31}^{*2} \frac{\tan(\omega l / 2 v_{11}^{E*})}{\omega l / 2 v_{11}^{E*}} \right] \quad (7)$$

Where ε_{33}^{X*} is complex intensive (stress-free) relative permittivity, v_{11}^{E*} is complex sound velocity, which is defined as $v_{11}^{E*} = 1/\sqrt{\rho s_{11}^{E*}}$ with mass density ρ and complex intensive (E -constant) elastic compliance s_{11}^{E*} , and k_{31}^* is complex electromechanical coupling coefficient, which is defined as $k_{31}^{*2} = d_{31}^{*2}/(\varepsilon_0 \varepsilon_{33}^{X*} s_{11}^{E*})$, with complex piezoelectric coefficient d_{31}^* .

ε_{33}^X and corresponding dielectric loss ($\tan \delta'_{33}$) can be determined from off-resonance capacitance and phase lag measurement, respectively. s_{11}^E and corresponding elastic loss ($\tan \phi'_{11}$) can be determined with the following equations from admittance resonance spectrum:

$$s_{11}^E = \frac{1}{4\rho f_A^2 l^2} \quad (8)$$

$$\tan \phi'_{11} = \frac{1}{Q_A} \quad (9)$$

Resonance (f_A) and antiresonance frequency (f_B) are maximum admittance and impedance point, respectively. Q_A and Q_B , which are corresponding mechanical quality factors, can be determined by 3 dB method[17] or quadrantal bandwidth method[27]. Electromechanical coupling factor, k_{31} , is determined by the following equation:

$$\frac{k_{31}^2}{1 - k_{31}^2} = \frac{\pi f_B}{2 f_A} \tan\left(\frac{f_B - f_A}{f_A}\right) \quad (10)$$

After ε_{33}^X , s_{11}^E and k_{31} are obtained, d_{31} can be obtained using the following equation:

$$d_{31}^2 = k_{31}^2 (\varepsilon_0 \varepsilon_{33}^X s_{11}^E) \quad (11)$$

Finally, intensive piezoelectric loss ($\tan \theta'_{31}$) can be determined by using the following equation:

$$\tan \theta'_{31} = \frac{\tan \delta'_{33} + \tan \phi'_{11}}{2} + \frac{1}{4} \left(\frac{1}{Q_A} - \frac{1}{Q_B} \right) \left[1 + \left(\frac{1}{k_{31}} - k_{31} \right)^2 \Omega_B^2 \right] \quad (12)$$

Where k_{31} is real part of complex electromechanical coupling factor and Ω_B is normalized antiresonance frequency, which is represented in terms of antiresonance angular frequency defined by $\omega_B = 2\pi f_B$ and s_{11}^E -related sound velocity (v_{11}^E):

$$\Omega_B = \frac{\omega_B l}{2v_{11}^E} \quad (13)$$

The electromechanical coupling square loss, imaginary part of k_{31}^{*2} , can be determined by the following equation:

$$\tan \chi_{31} = 2 \tan \theta'_{31} - \tan \delta'_{33} - \tan \phi'_{11} \quad (14)$$

With Standard k_{31} specimen, the only real extensive parameter that can be obtained is extensive elastic compliance (s_{11}^D), which is defined as:

$$s_{11}^D = s_{11}^E (1 - k_{31}^2) \quad (15)$$

Extensive (strain-free) dielectric permittivity (ϵ_{33}^x) can be obtained from the damped capacitance with thickness-mode (k_t) plate, by measuring admittance spectrum around the fundamental resonance frequency. However, since the measurement accuracy is low in high frequency region, especially in MHz regime, researchers indirectly calculate ϵ_{33}^x by using complicated equations originated from piezoelectric constitutive relations[31].

All the loss parameters, which can be determined from the equations in section 3.1, are intensive losses. In order to obtain extensive loss, one must utilize the following matrix equation[17]:

$$\begin{bmatrix} \tan \delta' \\ \tan \phi' \\ \tan \theta' \end{bmatrix} = [K] \begin{bmatrix} \tan \delta \\ \tan \phi \\ \tan \theta \end{bmatrix} \quad (16)$$

Where $[K]$ is 3×3 matrix that is called $[K]$ matrix, which is defined as:

$$[K] = \begin{bmatrix} 1 & k^2 & -2k^2 \\ k^2 & 1 & -2k^2 \\ 1 & 1 & -1 - k^2 \end{bmatrix} \quad (17)$$

$[K]$ is involutory ($[K] = [K]^{-1}$), so that inverse relationship of Equation (16) should also hold. It is noteworthy to mention that the $[K]$ matrix relationship Equation (16) is valid only for k_{31} type, not for k_{33} type. Pure extensive loss for k_{33} mode type can rather be obtained in 3D constrained conditions.

So far, physical parameter determination process of both intensive and extensive parameters for the Standard k_{31} mode has been discussed. It is noteworthy to mention that obtaining extensive parameters requires additional steps. Furthermore, from k -matrix formulation, it should be noted that the errors for extensive losses become larger due to error propagation.

3.2 Parameter Determination Using Standard k_{33} Mode

For k_{33} mode, the admittance equation is given by:

$$Y_{33}^* = \frac{j\omega w t \varepsilon_0 \varepsilon_{33}^{X*} (1 - k_{33}^{*2})}{l \left[1 - k_{33}^{*2} \frac{\tan(\omega l / 2v_{33}^{D*})}{\omega l / 2v_{33}^{D*}} \right]} \quad (18)$$

where k_{33}^{*2} is electromechanical coupling factor defined as $k_{33}^{*2} = d_{33}^{*2} / (\varepsilon_0 \varepsilon_{33}^{X*} s_{33}^{E*})$ and v_{33}^{D*} is extensive elastic compliance (s_{33}^{D*})-related sound velocity; dimension is defined in Figure 1 (b). ε_{33}^{X*} can also be measured with Standard k_{33} specimens; however, because of intrinsic geometry, ε_{33}^{X*} measured from k_{33} specimens are normally overestimated depending on the sample's aspect ratio[18,25,26,32]. Therefore, to obtain ε_{33}^{X*} , either Standard k_{31} specimens or thickness mode plates should be utilized.

The admittance equations of k_{31} mode and k_{33} mode have different resonance conditions, as well as different electrical boundary conditions. For instance, k_{31} mode has E -

constant condition because of free charges due to surface electrode that cancels out depolarization field, whereas k_{33} mode, which has D -constant condition, does not have any free charges that cancel out the depolarization field [10]. Due to different electrical boundary conditions that affects elasticity, they also have different resonance conditions: From Eq. (7), $Y_{31}^* = \infty$ when $\tan(\omega l/2v_{11}^{E*}) = \infty$, whereas Eq. (17) gives $Y_{33}^* = 0$ when $\tan(\omega l/2v_{33}^{D*}) = \infty$. Therefore, different from k_{31} mode, in which elastic compliance is obtained from resonance frequency, k_{33} mode has a half-wave resonating condition at the antiresonance frequency, and s_{33}^D is obtained with the following equation:

$$s_{33}^D = \frac{1}{4\rho f_B^2 l^2} \quad (19)$$

The complex elastic constants of k_{33} mode (s_{33}^{D*}) is not perfectly D -constant, due to mechanical boundary condition. Assuming 3 is direction along l and 1 and 2 are along t and w , respectively (see Figure 1 (b)), and l is much larger than w and t , the condition $X_1 = X_2 = 0$ satisfies, meaning that there is no depolarization field along 1 and 2 directions. Since it is the case, k_{33} mode specimen has E -constant in those directions. In 3D notation proposed by Ikeda [27], the elastic compliance is given by s_{33}^{EED*} , which means E_1 , E_2 and D_3 are constant. Therefore, the imaginary part of s_{33}^{D*} is represented as triple-prime loss ($\tan \phi_{33}'''$), to be distinguished from purely extensive loss ($\tan \phi_{33}$). $\tan \phi_{33}'''$ is obtained from Q_B of k_{33} mode and defined by the following expression:

$$\tan \phi_{33}''' = \frac{1}{Q_B} = \frac{1}{1 - k_{33}^2} [\tan \phi_{33}' - k_{33}^2 (2 \tan \theta_{33}' - \tan \delta_{33}')] \quad (20)$$

Note that Equation (20) follows the $[K]$ matrix, but the relationship is between triple-prime and single-prime, not between non-prime and single-prime losses. Similar to k_{31} mode, electromechanical coupling factor for k_{33} mode can be determined with f_A and f_B :

$$k_{33}^2 = \frac{\pi f_A}{2 f_B} \tan\left(\frac{f_B - f_A}{f_B}\right) \quad (21)$$

Different from k_{31} mode, intensive elastic compliance (s_{33}^E) can be indirectly obtained from the following equation:

$$s_{33}^E = \frac{s_{33}^D}{(1 - k_{33}^2)} \quad (22)$$

In order to obtain intensive elastic loss ($\tan \phi'_{33}$) and intensive piezoelectric loss ($\tan \theta'_{33}$), the following two equations should be utilized:

$$\tan \phi'_{33} - 2k_{33}^2 \tan \theta'_{33} = \frac{(1 - k_{33}^2)}{Q_{B,33}} - k_{33}^2 \tan \delta'_{33} \quad (23)$$

$$\begin{aligned} & \tan \phi'_{33} + 2 \tan \theta'_{33} \\ &= -\left(\frac{1}{Q_{A,33}} - \frac{1}{Q_{B,33}}\right) \frac{(k_{33}^2 - 1 + \Omega_{A,33}^2/k_{33}^2)}{2} - \tan \delta'_{33} \end{aligned} \quad (24)$$

$\tan \phi_{33}$ and extensive piezoelectric loss ($\tan \theta_{33}$) cannot be obtained directly with k_{33} mode specimen, but rather can be obtained by measuring k_t mode plate. Since k_t mode plates have nonzero stress along 1 and 2 directions (two orthogonal directions that are both perpendicular to polarization), there exist depolarization field along those directions; therefore, with 3D notation, the elastic stiffness is c_{33}^{DDD*} and the corresponding loss is $\tan \phi_{33}$.

By now, the method to obtain different real and imaginary parameters using Standard k_{31} and k_{33} mode has been discussed. In usual case, the parameters that are not directly determined from resonance frequencies and quality factors, but rather determined from the equations with other physical parameters, have larger statistical errors due to error propagation process. To the extreme, Zhuang[31] reported 100 % statistical error on $\tan \theta_{33}$ on a soft PZT.

3.3 Analytical Admittance Equation of PE configuration

The derivation process for analytical admittance equation of the PE configuration has

already been discussed in our previous papers [29]. If the admittance equation is simplified, the universal admittance equation is given by:

$$Y_{PE} = j\omega \left[\frac{2d_{31}^{*2} v_{11}^{E*} v_{side}^* s_{side}^*}{ts_{11}^{E*} \left[\frac{s_{side}^* v_{side}^*}{\tan\left(\frac{a\omega l}{2v_{11}^{E*}}\right)} - v_{11}^{E*} s_{11}^{E*} \tan\left(\frac{(1-a)\omega l}{2v_{side}^*}\right) \right]} + \frac{al\omega \varepsilon_0 \varepsilon_{33}^{X*} (1 - k_{31}^{*2})}{t} \right] \quad (25)$$

Where a is portion of center part ($0 < a < 1$), s_{side}^* is elastic compliance of side part along the length and v_{side}^* is sound velocity along the length of side part. Depending on the electrical boundary or poling conditions of side part, s_{side}^* can be s_{11}^{D*} (k_{31} NE), s_{33}^{D*} (k_{33} OC) or s_{33}^{E*} (k_{33} SE), and the corresponding elastic loss (imaginary part) values in the complex notation are $\tan \phi_{11}$, $\tan \phi_{33}'''$, and $\tan \phi_{33}'$, respectively. In Equation (25), the first term involving tangent functions is combined motional admittance, and the second term is damped admittance. The damped admittance is identical to that of k_{31} mode specimen in Equation (7), with different length (al , because only center portion is considered).

For motional admittance part in Equation (25), taking out $\frac{d_{31}^{*2}}{s_{11}^{E*2}}$ term outside the square bracket, then making numerator 1 by dividing both numerator and denominator by numerator, and using the fact that $v \times s = \frac{1}{\rho v}$, we obtain:

$$Y_{m,PE} = \frac{j\omega}{t} \frac{2d_{31}^{*2}}{s_{11}^{E*2}} \left[\frac{1}{\left[\rho v_{11}^{E*} \cot\left(\frac{a\omega l}{2v_{11}^{E*}}\right) - \rho v_{side}^* \tan\left(\frac{(1-a)\omega l}{2v_{side}^*}\right) \right]} \right] \quad (26)$$

For simplicity, it is useful to discuss impedance form of Equation (26), which is:

$$Z_{m,PE} = \frac{-jt}{2w} \frac{s_{11}^{E*2}}{d_{31}^{*2}} \left[\rho v_{11}^{E*} \cot\left(\frac{a\omega l}{2v_{11}^{E*}}\right) - \rho v_{side}^* \tan\left(\frac{(1-a)\omega l}{2v_{side}^*}\right) \right] \quad (27)$$

Equation (27) shows clear separation of motional impedance for center and side part. Including multiplication term outside the square bracket, the first term inside the square bracket with cotangent function is impedance of the center part and the second term with tangent function is impedance of the side part. To confirm the equation, $a = 1$ can be put into the equation. In the case of $a = 1$, the center part takes 100 % of the entire geometry, so the equation describes Standard k_{31} mode, and Equation (25) turns into Equation (7). In the case of a approaches to zero, resonance frequencies and mechanical quality factors in an admittance curve approaches to reflect elasticity of side part.

3.4 Parameter Determination Process Using Standard k_{31} and PE Specimens

The following steps are parameter determination process using Standard k_{31} mode samples and PE samples:

1. The dimensions (l, w, t), mass (ρ) and the center portion (a) for PE should be measured for each sample. This procedure is always required for any piezoelectric specimen measurement.
2. Admittance curves of Standard k_{31} mode samples should be measured, and related parameters ($s_{11}^{E*}, \varepsilon_{33}^X, d_{33}^*, k_{31}^*$) are obtained by using the equations shown in 3.1.1. Unlike Standard k_{33} mode specimens that have several issues, Standard k_{31} mode specimens do not have particular issues.
3. Admittance curves of PE specimens (k_{31} NE, k_{33} OC and k_{33} SE) should be measured, and elastic parameters are obtained with nonlinear regression curve fitting. Since the center portion of the PE specimens is k_{31} mode, k_{31} mode-related parameters exist in analytical solutions of PE configuration, as the form of damped and motional admittance. In order to minimize the fitting variables, intensive parameters determined from k_{31} mode in step 2 can be plugged into analytical solution when the fitting is

performed. Therefore, for each PE specimen, there are only 2 parameters (elastic compliance and corresponding elastic loss of side part) that are needed to be determined.

It is noteworthy to mention that Majzoubi *et al.*[17] proved 1D assumption $s_{11}^{D*} \approx 1/c_{11}^{D*}$ holds; therefore, the imaginary part of s_{11}^{D*} is purely extensive loss ($\tan \phi_{11}$).

4. k_{33} and d_{33} can be determined from the following equations, after s_{33}^D and s_{33}^E are determined from k_{33} OC and k_{33} SE, respectively:

$$k_{33} = \sqrt{1 - \frac{s_{33}^D}{s_{33}^E}} \quad (28)$$

$$d_{33} = k_{33} \sqrt{\varepsilon_0 \varepsilon_{33}^X s_{33}^E} \quad (29)$$

These parameters, according to IEEE Standard[24], are determined from Standard k_{33} mode specimens. However, with Standard k_{33} mode specimens, reliable data cannot be obtained, because there are several issues, such as high impedance values near antiresonance frequency that causes huge noise in experimental admittance/impedance curves, indispensable wire attachment that shifts antiresonance frequency, and fringing electric field issue due to intrinsic geometry. Therefore, With the aid of PE specimens, these parameters can be obtained more reliably.

5. Finally, $\tan \theta'_{33}$ and $\tan \chi_{33}$ can be determined using the following equation[31]:

$$\tan \theta'_{33} = \frac{1}{2k_{33}^2} [\tan \phi'_{33} - (1 - k_{33}^2) \tan \phi'''_{33} + k_{33}^2 \tan \delta'_{33}] \quad (30)$$

$$\tan \chi_{33} = 2 \tan \theta'_{33} - \tan \delta'_{33} - \tan \phi'_{33} \quad (31)$$

So far, determination method of all the intensive parameters and extensive-like elastic parameters of k_{31} and k_{33} mode has been discussed, with combination of Standard k_{31} mode and three PE samples. As already mentioned in section 3.2, other extensive parameters cannot solely be obtained from k_{31} and k_{33} mode but obtained by measuring k_t mode samples. Figure

4 summarizes parameter determination process using Standard k_{31} mode and three PE samples.

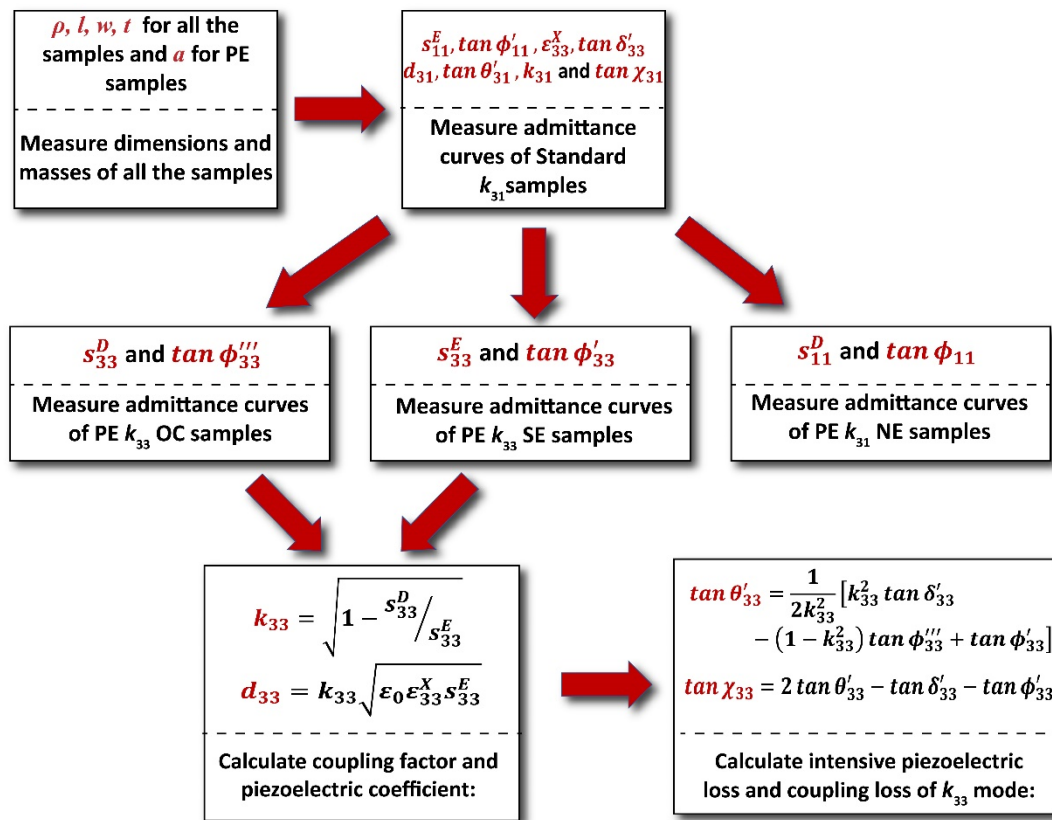


Figure 4. Parameter determination process using Standard k_{31} and three types of PE samples.

3.5 Simplification of PE Configuration

In both Majzoubi *et al.*[17] and our previous work[18], both k_{31} and k_{33} PE configurations included open circuit (OC) and short circuit (SC). In the case of k_{31} mode PE, this inclusion was necessary to characterize both resonance and antiresonance frequencies and corresponding mechanical quality factors; in the case of k_{33} mode PE, SC specimen was necessary to obtain d_{33} and $\tan \theta_{33}'$. However, in this study, some of the PE geometries are omitted for the following reasons:

1. Since Standard k_{31} mode does not have particular issues, OC (for antiresonance characterization) and SC (for resonance characterization) of k_{31} PE are not needed.

Including two geometry brings out redundant tasks. Only geometry needed for k_{31}

PE is NE, since it allows direct determination of extensive elastic compliance and extensive elastic loss.

2. For k_{33} mode PE, SC was omitted, because of complicated process to obtain d_{33} and $\tan \theta'_{33}$. In order to obtain these parameters using SC specimen, s_{33}^{D*} and s_{33}^{E*} should be determined first and plugged into very complicated analytical admittance equation[18,29]. Furthermore, attaching wires to SC specimens possibly distort experimental admittance/impedance curves, as soldering iron and wires can add the mass to the specimens. Without using SC specimens, d_{33} and $\tan \theta'_{33}$ can be obtained by using Equation (29) and (30), after determination of s_{33}^{D*} and s_{33}^{E*} from k_{33} PE OC and k_{33} PE SE, respectively.
3. Reducing types of samples would greatly accelerate sample preparation, measurement, and analysis process.

Therefore, with omitted OC and SC for k_{31} mode PE and SC for k_{33} mode PE, the modified PE method includes NE for k_{31} mode PE, OC and SE for k_{33} mode PE, along with Standard k_{31} specimen.

4. Results

4.1 Possible Error Causes of PE Specimens

In this section, the factors, some of which are demonstrated with FEA simulation results, that possibly causes the error for PE specimens will be discussed. Those factors can be fringing electric field at center part, and partial poling issue near the boundary between center and side part.

4.1.1 Fringing Electric Field Occurring at the Center Part

The analytical solutions for PE configurations were already verified with FEA in previous works[29]. Previously, the differences between admittance equations of analytical solutions and FEA were discussed: the height (baseline) difference and peak values[29]. With basic intuition, it is noticed that the center portion must experience fringing electric field, due to the fact that it is surrounded with side part that has similar magnitude of dielectric permittivity. In order to profoundly investigate what may cause the differences, FEA simulation was performed. Table 1 shows the input ϵ_{33}^X used in the simulation, along with ϵ_{33}^X determined from center portion's impedance value generated by simulation of each PE. Somehow, in the case of k_{33} PE SE, the electrode on the side part may suppress the fringing electric field, so almost no change occurs in ϵ_{33}^X . However, in the case of both k_{31} PE NE and k_{33} PE OC, significant overestimation of ϵ_{33}^X is observed, though smaller value was used as input for the simulation. We also reported overestimation of ϵ_{33}^X obtained from center part of PE samples[16]. Therefore, in order to minimize the difference, the overestimated values of ϵ_{33}^X is used for analytical solutions, rather than the same input FEA parameter, in order to calibrate the overestimation of ϵ_{33}^X at the center portion. Figure 5 shows analytical and FEA admittance curves of k_{31} PE NE and k_{33} PE OC, with and without permittivity calibration. Without calibration, the height (baseline) difference is obvious, whereas the height of admittance curves with the calibration shows much better agreement between analytical solutions and FEA. Since degree of overestimation is different from each sample due to different a , ϵ_{33}^X should be directly measured from the center part of each sample and used as fitting parameter, rather than using ϵ_{33}^X determined from Standard k_{31} plate. The remaining small difference in peak values may be due to the difference between 1D consideration of analytical solution and 3D consideration of FEA. Despite the differences in peak values, less than 0.3 % difference occurs for resonance frequencies, and less than 1.6 % difference occurred for quality factors.

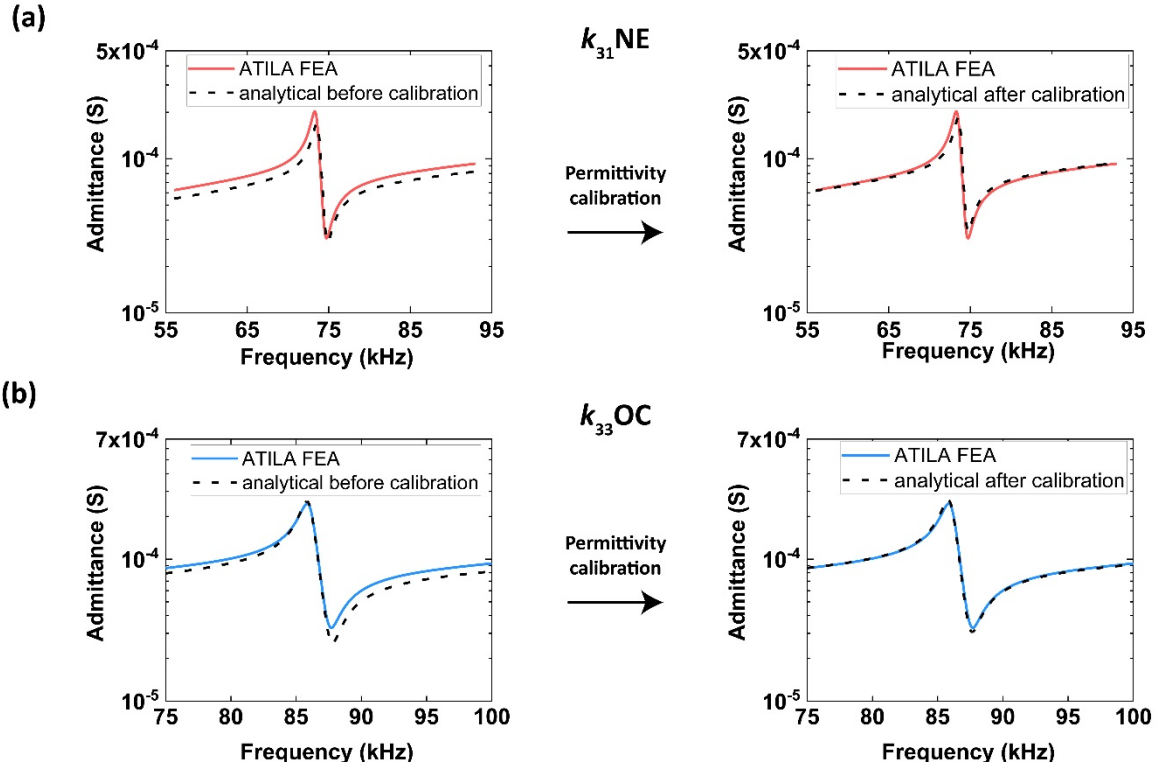


Figure 5. Admittance curves generated from ATILA FEA, and analytical solution with and without permittivity calibration of (a)PE k_{31} NE and (b) PE k_{33} OC.

ϵ_{33}^X values from ATILA FEA

Input	Output from k_{31} PE	Output from k_{33} PE	Output from k_{33} PE
	NE center	OC center	SE center
1700	1872	1918	1707

Table 1. ϵ_{33}^X used as input the simulation (PZT 5A), along with ϵ_{33}^X determined from center portion's impedance values generated by simulation of each PE for comparison.

4.1.2 Partial Poling Issues in k_{33} PE Specimens

For k_{33} PE OC and k_{33} PE SE, two-step poling process is involved: bulk ceramic is poled, then cut into thin plates with desired sample dimension, center part of each piece is electroded and re-poled. The process is required, since the side part should have polarization along the length direction for k_{33} mode elastic characterization, whereas the center actuation part should always be k_{31} mode, having polarization along thickness direction. However, in the process of two-step poling with two different directions, canted poling may occur at the boundary between center and side part. Since the part with canted polarization has different physical properties compared to upward and side polarization, it would affect experimental admittance curve.

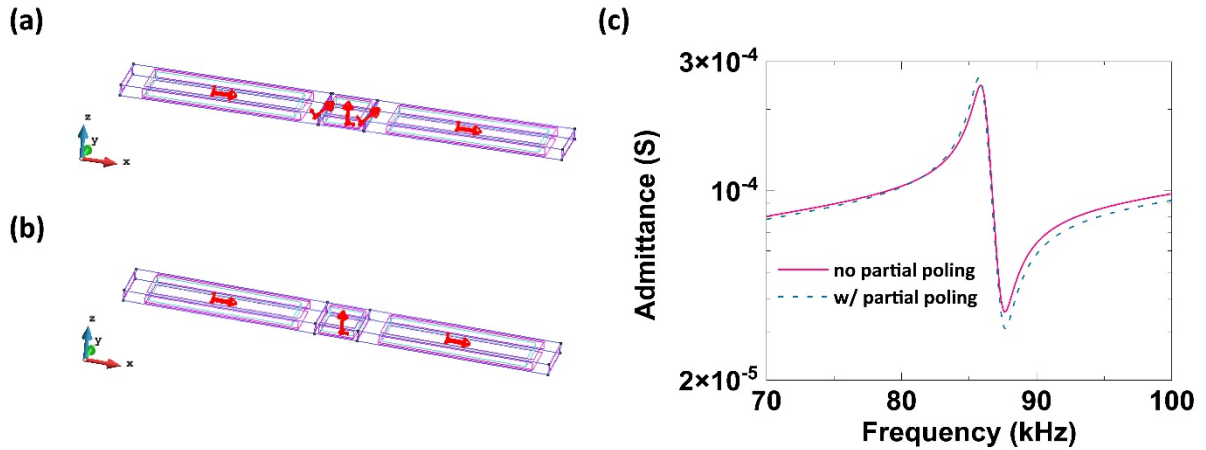


Figure 6. ATILA FEA geometry for (a) PE with partial poling (45° at the interface of side and center) and (b) without partial poling. (c) Admittance curve difference between two cases.

In order to investigate the effect of canted polarization, ATILA FEA simulation was performed. Two volumes, each of which has $50\ \mu\text{m}$ gap in the length direction with 45° canted polarization, were located at each end of the center portion in PE geometry, as shown in Figure 6 (a) and (b). Figure 6 (c) shows the comparison of admittance spectra of two cases: PE geometry with and without the volumes with canted polarization. Even though volumes with canted polarization were inserted in both edge of the center portion, the admittance curve does

not show significant difference, when compared to the admittance curves of PE without the volumes with canted polarization. In order to make quantitative comparison, f_A , f_B , Q_A and Q_B of two admittance curves are compared. Table 2 shows the values of these parameters, along with the percentage differences. The percentage difference in frequency values (f_A and f_B) ranges from 0.1 % to 0.2 %, and the difference in quality factors (Q_A and Q_B) ranges from 0.26 – 0.4 %. Therefore, partial canted polarization that may be occurred at the boundary between center and side part does not significantly affect measured admittance curves, when considering FEA simulation results.

	f_a (KHz)	Q_a ...	f_b (KHz)	Q_b ...
w/o partial poling	86.1	76.9	87.4	83.7
w/ partial poling	85.9	76.7	87.5	84.1
Difference (%)	0.2 %	0.26 %	0.1 %	0.4 %

Table 2. values of f_A , f_B , Q_A and Q_B and percentage difference in the cases of with and without partial poling volumes in k_{33} PE OC with input parameters of PZT 5A.

4.2 Parameter Determination

Table 3 shows parameters determined from PE fitting method. The real and imaginary parameters determined from k_{31} mode samples (See supplementary materials for k_{31} mode parameters) were used to minimize fitting variables, and permittivity calibration discussed in section 4.1.1 was also applied. The fitting curves, along with experimental admittance curves, near resonance and antiresonance peaks are shown in Figure 7 (Fittings of full curves are shown in supplementary materials). All the percentage fitting errors were less than 1 %, which represents great fit of analytical solutions to experimental admittance curves. In table 5, in terms of statistical variation, PE samples show similar error range, compared to Standard k_{31}

samples. Therefore, PE method is as reliable as standard method. The values in Table 3 have slight discrepancies when compared to physical parameter values of PIC 255 in our previous report[18]. This may be due to that they were made from different ceramic blocks, as well as difference in electrode materials.

Parameters determined from PE samples

PIC 181				
Real Parameters				
s_{11}^D ($\times 10^{-12} \text{ m}^2/\text{N}$)	s_{33}^D ($\times 10^{-12} \text{ m}^2/\text{N}$)	s_{33}^E ($\times 10^{-12} \text{ m}^2/\text{N}$)	d_{33} (pC/N)	k_{33}
10.53 ± 0.05	8.53 ± 0.04	13.03 ± 0.06	224 ± 2	0.588 ± 0.004
Imaginary Parameters				
$\tan \phi_{11}$ (%)	$\tan \phi_{33}'''$ (%)	$\tan \phi_{33}'$ (%)	$\tan \theta_{33}'$ (%)	$\tan \chi_{33}$ (%)
0.039 ± 0.001	0.030 ± 0.001	0.053 ± 0.002	0.229 ± 0.003	0.043 ± 0.007
PIC 255				
Real Parameters				
s_{11}^D ($\times 10^{-12} \text{ m}^2/\text{N}$)	s_{33}^D ($\times 10^{-12} \text{ m}^2/\text{N}$)	s_{33}^E ($\times 10^{-12} \text{ m}^2/\text{N}$)	d_{33} (pC/N)	k_{33}
14.30 ± 0.05	9.68 ± 0.03	17.48 ± 0.1	365 ± 5	0.668 ± 0.001
Imaginary Parameters				
$\tan \phi_{11}$ (%)	$\tan \phi_{33}'''$ (%)	$\tan \phi_{33}'$ (%)	$\tan \theta_{33}'$ (%)	$\tan \chi_{33}$ (%)
0.87 ± 0.01	0.51 ± 0.01	1.19 ± 0.01	1.79 ± 0.02	0.85 ± 0.04

Table 3. Real and imaginary parameters of PIC 181 and PIC 255 determined from PE method.

Errors are from data variation of 6 samples.

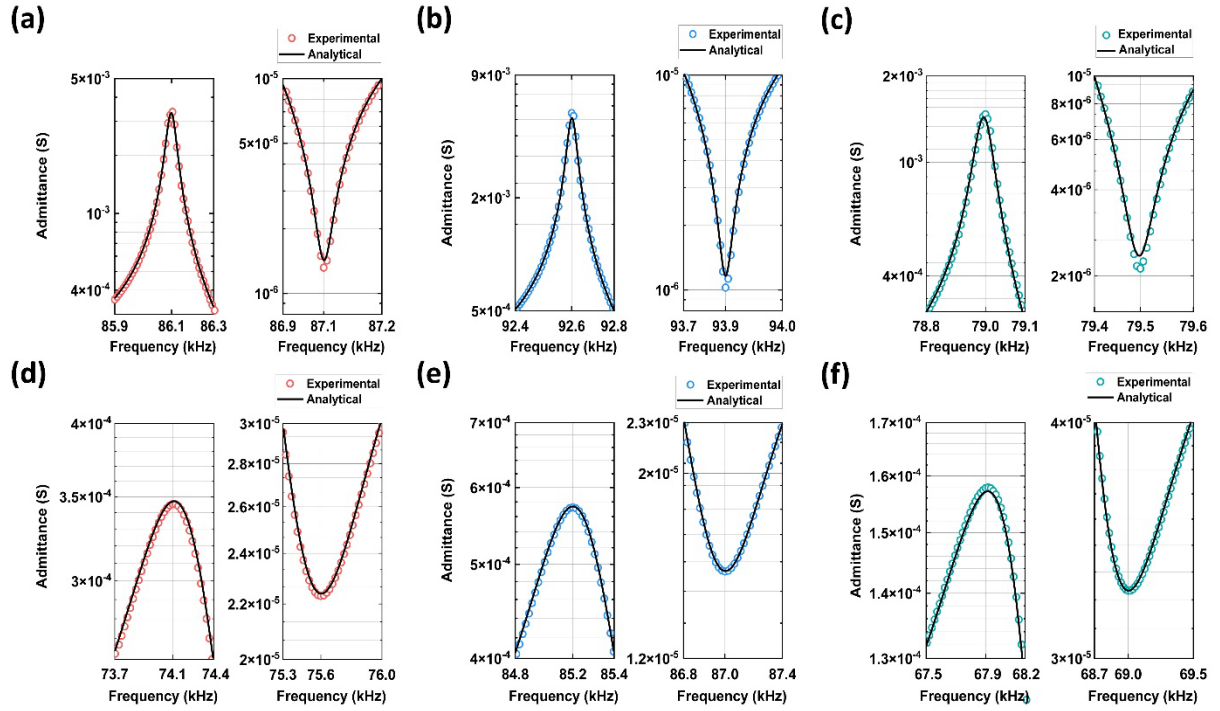


Figure 7. Experimental admittance curves of PE samples made of PIC 181 and PIC 255 measured with impedance analyzer. Black lines are analytical fitting curves.

5. Discussion

5.1 Benefits of PE Configuration as a Tool for Parameter Characterization

5.1.1 Tool for Extensive Elastic Loss Characterization for k_{31} mode

As aforementioned, Standard k_{31} mode does not have issues when being utilized for parameter determination. PE configuration (k_{31} NE) was proposed because it allows direct determination of extensive elastic compliance (s_{11}^D) and extensive elastic loss ($\tan \phi_{11}$). In order to obtain s_{11}^D and $\tan \phi_{11}$ with only Standard k_{31} mode specimen, Equation (15), (16) and (17) must be applied. Though error propagation process may not exaggerate the error of s_{11}^D so significantly, the error for $\tan \phi_{11}$ becomes enlarged, due to complicated $[K]$ matrix

equation. When expanded, the k -matrix provides the following equation for $\tan \phi_{11}$:

$$\tan \phi_{11} = \frac{1}{1 - k_{31}^2} (k_{31}^2 \tan \delta'_{33} + \tan \phi'_{11} - 2k_{31}^2 \tan \theta'_{31}) \quad (32)$$

With Equation (32), it is noteworthy to mention that, if $\tan \phi_{11}$ is obtained with Standard k_{31} mode, the error for k_{31} , $\tan \delta'_{33}$, $\tan \phi'_{11}$, and $\tan \theta'_{31}$ are all accumulated to $\tan \phi_{11}$. PE method proposed in this study, on the other hand, provides $\tan \phi_{11}$ (from curve fitting) that has an error comparable with $\tan \phi'_{11}$, which is directly determined from Q_A of Standard k_{31} mode specimen.

5.1.2 PE as Substitution for Standard k_{33} Specimen

Different from standard k_{31} specimen, standard k_{33} specimen has several issues that hinders researchers from obtaining accurate physical parameters. The most significant problem of standard k_{33} specimen is high impedance value near antiresonance frequency and corresponding 3 dB bandwidth.

Most impedance analyzers have accuracy limit near $10^7 - 10^8 \Omega$; above near $10^8 \Omega$, the measurement error becomes larger than 10 % [33-36]. Among 4 impedance analyzers that we investigated, Agilent 4294A Precision Impedance Analyzer has the lowest measurement error in the frequency regime from 1 KHz to 1 MHz, which corresponds to fundamental frequencies of most millimeter-scale IEEE Standard k_{31} and k_{33} samples. Figure 8 illustrates measurement error of Agilent 4294A Precision Impedance Analyzer, in terms of impedance and sweeping frequency [33]. As seen from Figure 8, from 100 Hz to 200 KHz, the measurement error exceeds 10 % at $4 \times 10^7 \Omega$. For the case of k_{33} mode specimen made from soft PZT, We previously reported impedance value about $2 \times 10^8 \Omega$ near antiresonance frequency and corresponding 3 dB bandwidth, along with large fluctuation (electrical noise) of impedance values [18]. Hard PZT, which has much larger mechanical quality factors than soft

PZT due to domain wall pinning, is likely to suffer more on low measurement accuracy near antiresonance frequency.

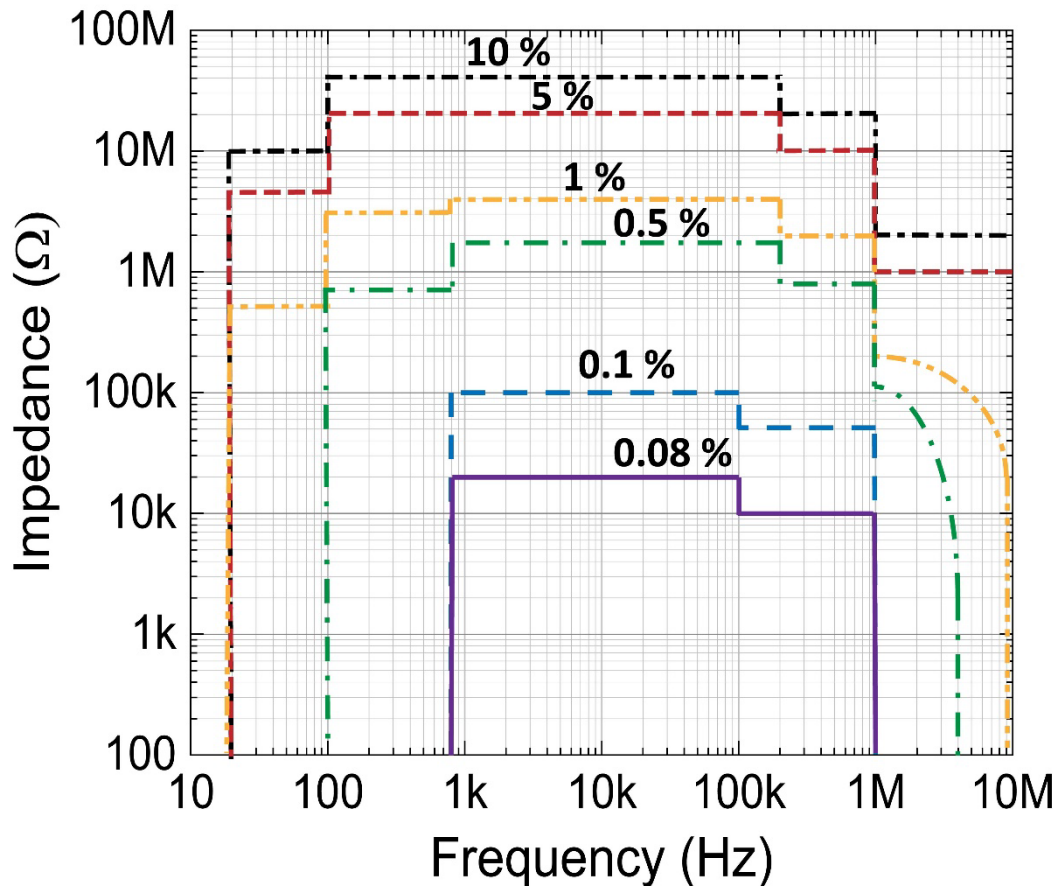


Figure 8. Measurement error in terms of impedance (in Ω) and operating frequency (in Hz) of Agilent 4294A Precision Impedance Analyzer. Redrawn from [29].

In order to see feasibility of impedance analyzer on k_{33} mode specimens made of various, and commonly utilized piezoelectric materials, FEA simulation was performed near antiresonance and corresponding 3 dB bandwidth; impedance values at antiresonance frequency and near 3 dB bandwidth for PZT 5A (soft), PZT 4 (semi-hard) and PZT 8 (hard) are shown in Table 4. For k_{33} mode geometry used for the simulation, dimension of $5 \times 5 \times 20$ mm (1 to 4 aspect ratio) was utilized, since the width to length aspect ratio of k_{33} mode specimens adapted by researchers range from 1:3 to 1:5[37-39]. The impedance values of PZT 5A near f_B

falls into measurement error range from 1 % to 5 %, which can be considered as okay values. However, those of PZT 4 fall into region of error more than 10 %, and those of PZT 8 are totally out of scope. Therefore, using k_{33} mode geometry for measurement with impedance analyzer is not appropriate.

	Impedance at f_B (Ω)	Impedance at 3 dB of f_B (Ω)
PZT 5A	7.35×10^6	5.20×10^6
PZT 4	7.15×10^7	5.05×10^7
PZT 8	2.07×10^8	1.46×10^8

Table 4. Impedance values at antiresonance frequency and 3 dB bandwidth for PZT 5A (soft), PZT 4 (semi-hard) and PZT 8 (hard), calculated from FEA simulation.

In terms of impedance analyzer's measurement accuracy, PE, on the other hand, provides much more reliable admittance/impedance values than Standard k_{33} mode specimen. It is noteworthy to mention that PIC 181, hard PZT used in this study, has $Q_m \sim 2000$, which is much larger than that of PZT 8 ($Q_m \sim 1000$). According to FEA results shown in Table 4 and Figure 8, even the impedance values near f_B and corresponding 3 dB bandwidth of PZT 8 is totally out of range; with even higher Q_m , reliable measurement near f_B is not possible for Standard k_{33} mode of PIC 181.

As shown in experimental admittance values in Figure 7, considering peak values, the admittance value of PIC 181 (hard PZT) ranges from 10^{-6} S to near 3×10^{-3} S, which corresponds to the range from $3.33 \times 10^2 \Omega$ to $10^6 \Omega$, and the admittance value of PIC 255 (soft PZT) ranges from 10^{-5} S to 5×10^{-4} S, which corresponds to the range from $2 \times 10^{-3} \Omega$ to $10^5 \Omega$. In accordance with Figure 8, The measurement error for PE samples made from hard PZT falls within 0.5 %, and that for samples made from soft PZT falls within 0.1 %. Compared to measurement error range out of scope for Standard Standard k_{33} mode, the measurement error

for PE samples less than 0.5 % is significantly smaller, and PE samples can effectively substitute Standard k_{33} mode specimens for parameter determination purpose.

6. Conclusion

In this study, detailed parameter determination process using samples with PE configuration, along with simplified PE admittance equations and possible error causes, has been discussed. The center part of PE is likely to undergo fringing electric field and proper calibration is needed during fitting process. It was shown that the possible errors that may come from the volumes with canted polarization and statistical variation that comes from the parameters determined from Standard k_{31} specimen are small (less than 0.2 %) enough to be neglected. With samples with PE configuration, researchers can obtain not only physical parameters with smaller statistical error by avoiding error propagation process, but also more reliable impedance/admittance curves from impedance analyzers. Accurate physical parameter values determined from PE are not only essential to elucidate heat dissipation mechanism of piezoelectric materials, but also necessary for accurate piezoelectric FEA simulation for prototype testing of piezoelectric devices. The physical meaning of the performance difference between hard and soft PZT will be report in the successive paper.

Acknowledgement

This work was supported by Office of Naval Research under Grant Number N00014-17-1-2088

References

- [1] A. Iula, F. Vazquez, M. Pappalardo, J.A. Gallego, Finite element three-dimensional analysis of the vibrational behaviour of the Langevin-type transducer, *Ultrasonics* 40(1-8) (2002) 513-517.
- [2] T. Nishimura, H. Hosaka, T. Morita, Resonant-type smooth impact drive mechanism (SIDM) actuator using a bolt-clamped Langevin transducer, *Ultrasonics* 52(1) (2012) 75-80.
- [3] E.M. Syed, F.P. Dawson, E.S. Rogers, Analysis and modeling of a Rosen type piezoelectric transformer, 2001 IEEE 32nd Annual Power Electronics Specialists Conference (IEEE Cat. No. 01CH37230), IEEE, 2001, pp. 1761-1766.
- [4] A.V. Mezheritsky, Quality factor concept in piezoceramic transformer performance description, *IEEE transactions on ultrasonics, ferroelectrics, and frequency control* 53(2) (2006) 429-442.
- [5] H. Fu, E.M. Yeatman, A miniaturized piezoelectric turbine with self-regulation for increased air speed range, *Appl. Phys. Lett.* 107(24) (2015) 243905.
- [6] H. Debeda, T. Freyhold, J. Mohr, U. Wallrabe, J. Wengelin, Development of miniaturized piezoelectric actuators for optical applications realized using LIGA technology, *Journal of microelectromechanical systems* 8(3) (1999) 258-263.
- [7] Y. Zhuang, S.O. Ural, A. Rajapurkar, S. Tuncdemir, A. Amin, K. Uchino, Derivation of piezoelectric losses from admittance spectra, *Jpn. J. Appl. Phys.* 48(4R) (2009) 041401.
- [8] K. Uchino, Y. Zhuang, S.O. URAL, Loss determination methodology for a piezoelectric ceramic: new phenomenological theory and experimental proposals, *J. Adv. Dielectr.* 1(01) (2011) 17-31.
- [9] X. Gao, J. Yang, J. Wu, X. Xin, Z. Li, X. Yuan, X. Shen, S. Dong, Piezoelectric actuators and motors: Materials, designs, and applications, *Advanced Materials Technologies* 5(1) (2020) 1900716.
- [10] K. Uchino, High-Power Piezoelectrics and Loss Mechanisms, *Advanced Piezoelectric Materials*, Elsevier 2017, pp. 647-754.
- [11] H. Daneshpajoo, M. Choi, Y. Park, T. Scholchwar, E. Hennig, K. Uchino, Compressive stress effect on the loss mechanism in a soft piezoelectric Pb (Zr, Ti) O₃, *Rev. Sci. Instrum.* 90(7) (2019) 075001.
- [12] J. Zheng, S. Takahashi, S. Yoshikawa, K. Uchino, J. De Vries, Heat generation in multilayer piezoelectric actuators, *J. Am. Ceram. Soc.* 79(12) (1996) 3193-3198.
- [13] Y.-H. Su, Y.-P. Liu, D. Vasic, W.-J. Wu, F. Costa, C.-K. Lee, Power enhancement of piezoelectric transformers by adding heat transfer equipment, *IEEE transactions on ultrasonics, ferroelectrics, and frequency control* 59(10) (2012) 2129-2136.
- [14] K. Uchino, S. Hirose, Loss mechanisms in piezoelectrics: how to measure different losses separately, *IEEE Transactions on Ultrasonics, ferroelectrics, and frequency control* 48(1) (2001) 307-321.
- [15] G. Liu, S. Zhang, W. Jiang, W. Cao, Losses in ferroelectric materials, *Materials Science and Engineering: R: Reports* 89 (2015) 1-48.
- [16] G. Arlt, Piezoelectric relaxation, *Ferroelectrics* 40(1) (1982) 149-157.
- [17] M. Majzoubi, H.N. Shekhani, A. Bansal, E. Hennig, T. Scholchwar, K. Uchino, Advanced methodology for measuring the extensive elastic compliance and mechanical loss directly in k31 mode piezoelectric ceramic plates, *J. Appl. Phys.* 120(22) (2016) 225113.
- [18] Y. Park, Y. Zhang, M. Majzoubi, T. Scholchwar, E. Hennig, K. Uchino, Improvement of the standard characterization method on k33 mode piezoelectric specimens, *Sensors and Actuators A: Physical* (2020) 112124.
- [19] K.S. Maxwell, J.D. Whitcomb, Z. Ounaies, A. Barhoumi, Finite element analysis of a three-phase piezoelectric nanocomposite, *J. Intell. Mater. Syst. Struct.* 21(11) (2010) 1073-1084.

- [20] M. Algueró, C. Alemany, L. Pardo, A.M. González, Method for obtaining the full set of linear electric, mechanical, and electromechanical coefficients and all related losses of a piezoelectric ceramic, *J. Am. Ceram. Soc.* 87(2) (2004) 209-215.
- [21] T. Meurisse, D. Damjanovic, Modeling losses of a piezoelectric resonator: Analytical vs finite elements analysis, 2017 Joint IEEE International Symposium on the Applications of Ferroelectric (ISAF)/International Workshop on Acoustic Transduction Materials and Devices (IWATMD)/Piezoresponse Force Microscopy (PFM), IEEE, 2017, pp. 71-74.
- [22] G. Arlt, H. Dederichs, Complex elastic, dielectric and piezoelectric constants by domain wall damping in ferroelectric ceramics, *Ferroelectrics* 29(1) (1980) 47-50.
- [23] R. Bechmann, I. Fair, IRE standards on piezoelectric crystals: Determination of the elastic, piezoelectric, and dielectric constants-the electromechanical coupling factor, *Proc. IRE* 46 (1958) 764-778.
- [24] A. Meitzler, H. Tiersten, A. Warner, D. Berlincourt, G. Couquin, F. Welsh III, IEEE standard on piezoelectricity, Society, 1988.
- [25] M. Hegg, A. Mamishev, Influence of variable plate separation on fringing electric fields in parallel-plate capacitors, Conference record of the 2004 IEEE International Symposium on Electrical Insulation, IEEE, 2004, pp. 384-387.
- [26] K. Pillai, Fringing field of finite parallel-plate capacitors, *Proceedings of the Institution of Electrical Engineers, IET*, 1970, pp. 1201-1204.
- [27] T. Ikeda, Fundamentals of piezoelectricity, Oxford University Press, Oxford ; New York, 1990.
- [28] Methods of Measurement for Piezoelectric Vibrators, IEEE Std 177 (1966).
- [29] Y. Park, M. Majzoubi, Y. Zhang, T. Scholehwar, E. Hennig, K. Uchino, Analytical modeling of k 33 mode partial electrode configuration for loss characterization, *J. Appl. Phys.* 127(20) (2020) 204102.
- [30] Y. Zhuang, S.O. Ural, K. Uchino, Methodology for characterizing loss factors of piezoelectric ceramics, *Ferroelectrics* 470(1) (2014) 260-271.
- [31] Y. Zhuang, Loss phenomenology and the methodology to derive loss factors in piezoelectric ceramics, (2011).
- [32] M. Hosseini, G. Zhu, Y.-A. Peter, A new formulation of fringing capacitance and its application to the control of parallel-plate electrostatic micro actuators, *Analog Integrated Circuits and Signal Processing* 53(2-3) (2007) 119-128.
- [33] Agilent 4294A Precision Impedance Analyzer Data Sheet, Agilent Technologies Inc., Santa Clara, CA, 2008.
- [34] Hioki IM3570 Impedance Analyzer Instruction Manual, Hioki E. E. Corporation, Nagano, Japan, 2012.
- [35] Zurich Instruments MFIA Impedance Analyzer User Manual, Zurich Instruments AG, Zurich, Switzerland, 2016.
- [36] Precision Impedance Analyzer 6500B Series User Manual, Wayne Kerr Electronics, West Sussex, UK, 2008.
- [37] M. Slabki, J. Wu, M. Weber, P. Breckner, D. Isaia, K. Nakamura, J. Koruza, Anisotropy of the high-power piezoelectric properties of Pb (Zr, Ti) O₃, *J. Am. Ceram. Soc.*
- [38] J. Peng, H. Luo, T. He, H. Xu, D. Lin, Elastic, dielectric, and piezoelectric characterization of 0.70 Pb (Mg_{1/3}Nb_{2/3}) O₃–0.30 PbTiO₃ single crystals, *Mater. Lett.* 59(6) (2005) 640-643.
- [39] H. Cao, V.H. Schmidt, R. Zhang, W. Cao, H. Luo, Elastic, piezoelectric, and dielectric properties of 0.58 Pb (Mg _{1/3} Nb _{2/3}) O ₃-0.42 PbTiO ₃ single crystal, *J. Appl. Phys.* 96(1) (2004) 549-554.

Supplementary Materials

for

Physical Parameters and Loss Determination of Piezoceramic Using Partial Electrode:

k_{31} and k_{33} mode cases

Yoonsang Park^{1,*}, Hossein Daneshpajoo¹, Timo Scholehwar², Eberhard Hennig², and Kenji Uchino¹

1) International Center for Actuators and Transducers (ICAT), The Pennsylvania State University, University Park, PA, 16802, USA

2) R&D Department, PI Ceramic GmbH, Lindenstrasse, 07589 Lederhose, Germany

1. ATILA FEA simulation conditions

1.1 FEA simulation of PE Geometry

The physical parameters of PZT 5A, which was already implemented in the software, were used for the simulation. $20 \times 2.5 \times 0.5$ mm = length \times width \times thickness geometry for PE configuration was drawn with the center part that takes 10 % (2 mm) of the entire length. The mesh numbers of 20, 4, and 4 were assigned for length, width, and thickness, respectively, for side part; mesh numbers of 5, 4, and 4 were assigned for center part. Figure S1 shows mesh geometry for FEA simulation. Since the fundamental frequency corresponds to the vibration along the length direction (x direction in Figure S1), we assigned more meshes in length and less meshes in the other directions, to reduce simulation time while maintaining simulation accuracy. Table S1 shows physical parameters of PZT 5A used FEA simulation. It should be noted that ATILA considers loss isotropy, so losses are denoted without subscripted direction notation. 1 V was assigned to one of the upper one of two faces (orthogonal to thickness), and ground was assigned to another face.

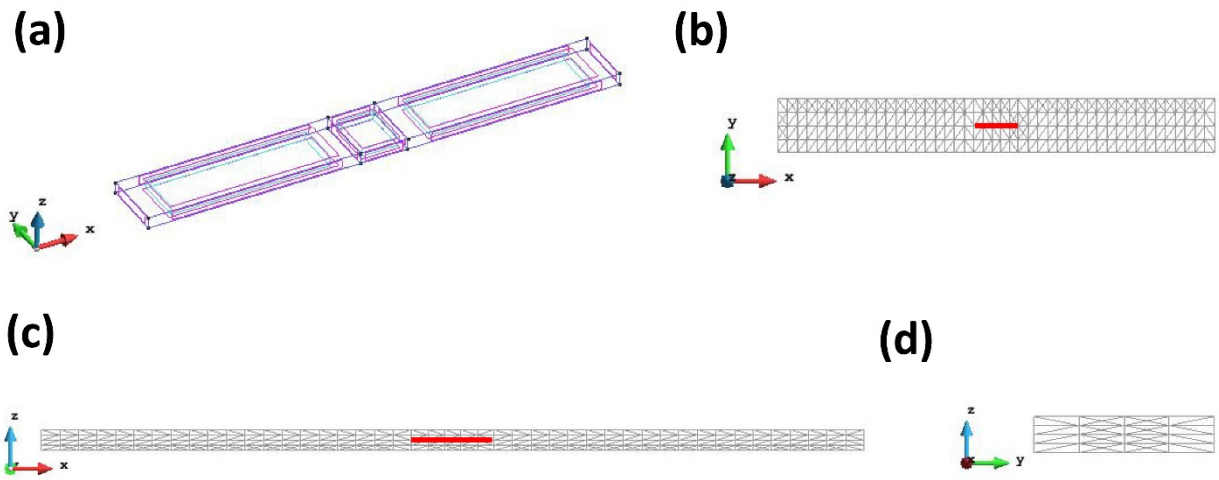


Figure S1. (a) PE geometry with coordinate in ATILA FEA and Mesh geometry for FEA simulation of PE configuration in (b) XY (c)XZ and (d) YZ plane. Red lines in (b) and (c) denote center part.

Density (kg/m ³)	7750		
relative permittivity	$\epsilon_{33}^X = 1700$	dielectric loss	$\tan \delta = 0.02$
elastic compliances (m ² /N)	$s_{11}^E = 16.4 \times 10^{-12}$ $s_{33}^E = 18.8 \times 10^{-12}$	elastic loss	$\tan \phi = 0.013$
piezoelectric constant (pC/N)	$d_{31} = -171$ $d_{33} = 374$	piezoelectric loss	$\tan \phi = 0.016$

Table S1. Physical parameter and loss values of PZT 5A used for FEA simulation

1.2 FEA Simulation of k_{33} Standard Geometry

In order to obtain impedance values near antiresonance frequency and corresponding 3 dB bandwidth for various, commercially available piezoelectric ceramics, k_{33} mode geometry

with PZT 5A (soft), PZT 4 (semi-hard) and PZT 8 (hard) with the dimension of $20 \times 5 \times 5$ mm = length \times width \times thickness (note that width and thickness have the same length). The mesh number was assigned to be 25,4 and 4 for length, width and thickness, respectively; the mesh geometry is schematically shown in Figure S2. 1 V was assigned to one of two faces orthogonal to the direction of polarization, and ground was assigned to the other face.

	PZT 4	PZT 8
mass density (kg/m ³)	7500	7600
relative permittivity (...)	$\epsilon_{33}^X = 1300$	$\epsilon_{33}^X = 1000$
elastic compliance (m ² /N)	$s_{33}^E = 15.5 \times 10^{-12}$	$s_{33}^E = 13.9 \times 10^{-12}$
Piezoelectric constant (pC/N)	$d_{33} = 289$	$d_{33} = 218$
dielectric loss	$\tan \delta = 0.004$	$\tan \delta = 0.004$
elastic loss	$\tan \phi = 0.002$	$\tan \phi = 0.001$
piezoelectric loss	$\tan \theta = 0.0035$	$\tan \theta = 0.003$

Table S2. Physical parameters and loss values of PZT 4 and PZT 8 used for FEA simulation.

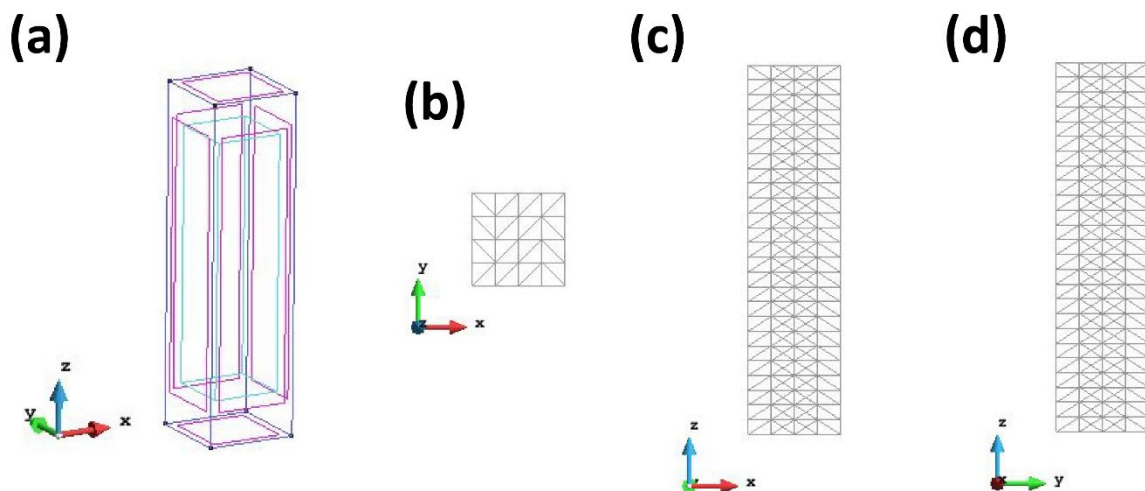


Figure S2. (a) PE geometry with coordinate in ATILA FEA and Mesh geometry for FEA simulation of PE configuration in (b) XY (c)XZ and (d) YZ plane.

2. Standard k_{31} mode parameters

Standard k_{31} mode samples made from PIC 181 and PIC 255 [PI Ceramic GmbH, Lederhose, Germany], with the dimension of $20 \times 2.5 \times 0.5$ mm, were prepared. The off-resonance and near-resonance admittance/impedance spectra of each sample were measured with 4294A Precision Impedance Analyzer [Agilent Technologies, Santa Clara, CA]. Table S3 shows determined physical parameters and losses from 6 samples (for each material). The error denotes standard error of the mean taken from standard variation among each sample and error propagation method.

Standard k_{31} Parameters			
PIC 181			
Real Parameters			
ε_{33}^X	s_{11}^E ($\times 10^{-12}$ m ² /N)	d_{31} (pC/N)	k_{31}
1263 \pm 3	11.94 \pm 0.03	-121.4 \pm 0.4	0.332 \pm 0.001
Imaginary Parameters			
$\tan \delta'_{33}$ (%)	$\tan \phi'_{11}$ (%)	$\tan \theta'_{31}$ (%)	$\tan \chi_{31}$ (%)
0.362 \pm 0.003	0.054 \pm 0.001	0.239 \pm 0.004	0.10 \pm 0.01
PIC 255			
Real Parameters			
ε_{33}^X	s_{11}^E ($\times 10^{-12}$ m ² /N)	d_{31} (pC/N)	k_{31}
1934 \pm 3	16.77 \pm 0.04	-194.7 \pm 0.5	0.363 \pm 0.003
Imaginary Parameters			
$\tan \delta'_{33}$ (%)	$\tan \phi'_{11}$ (%)	$\tan \theta'_{31}$ (%)	$\tan \chi_{31}$ (%)
1.54 \pm 0.01	1.21 \pm 0.02	2.26 \pm 0.04	1.8 \pm 0.1

Table S3. Physical parameters and losses determined from Standard k_{31} samples.

3. Experimental Admittance curves of PE samples

The full experimental admittance curves along with analytical fit of all types of PE specimens proposed in this study is shown in Figure S3. Note that the admittance curve agreement with analytical solution near resonance/antiresonance peak is in the main text.

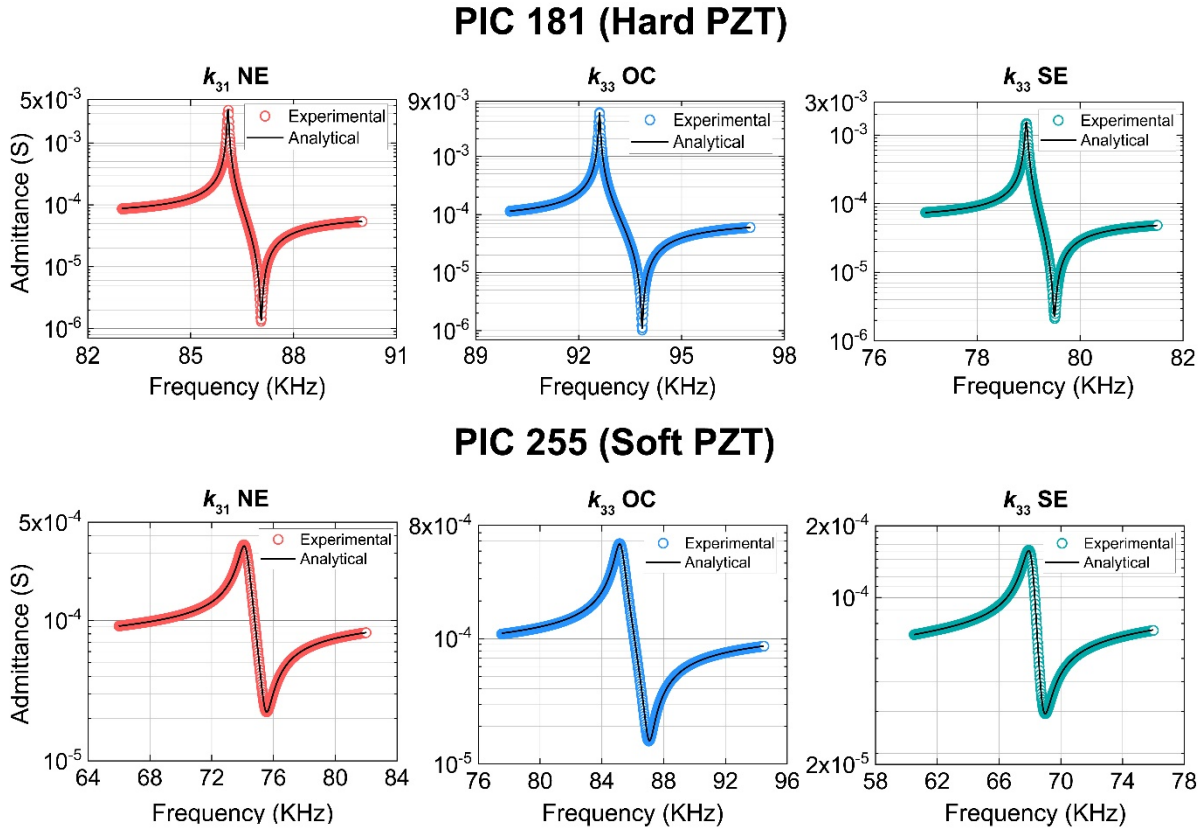


Figure S3. Full experimental admittance spectra of PE samples made of PIC 181 and PIC 255 measured with impedance analyzer. Black lines are analytical fitting curves.